Electrical characterization and conduction mechanism of impurity-doped $BaSi_2$ films grown on Si(111) by molecular beam epitaxy

M. Ajmal Khan[a], T. Saito[a], K. Nakamura[a], M. Baba[a], W. Du[a], K. Toh[a], K. Toko[a], and T. Suemasu[a,b,*]

[a]*Institute of Applied Physics, University of Tsukuba, Tsukuba, Ibaraki 305-8573, Japan*

[b]*Japan Science and Technology Agency, CREST, Chiyoda, Tokyo 102-0075, Japan*

The carrier concentrations and mobilities of impurity (Sb, In, Ga, Al, Ag, and Cu)-doped $BaSi_2$ films grown by molecular beam epitaxy on highly resistive *n*- or *p*-Si(111) substrates were measured at room temperature using the van der Pauw technique. Sb-, Ga- and Cu-doped $BaSi_2$ exhibited *n*-type conductivity, while In- Al- and Ag-doped $BaSi_2$ exhibited *p*-type conductivity. The temperature dependence of resistivity indicated that the carrier transport in Ga-, Al-, Ag-, and Cu-doped $BaSi_2$ is well explained by both Shklovskii-Efros-type and Mott-type variable range hopping conduction.

* E-mail: suemasu@bk.tsukuba.ac.jp

1. Introduction

The demand for cheaper energy imposes strict requirements on solar cell materials, such as a large absorption coefficient, a suitable bandgap to provide high conversion efficiency, and low cost. In the photovoltaic industry, almost 90% of solar cells are Si-based. However, the bandgap E_g, of crystalline Si is 1.1 eV at room temperature (RT), which is approximately 0.3 eV smaller than the ideal E_g of approximately 1.4 eV [1,2]. Optical absorption measurements have shown that the E_g value of $BaSi_2$ can be increased up to 1.4 eV by replacing half of the Ba atoms in $BaSi_2$ with isoelectric Sr atoms [3], which is in agreement with the theoretical result presented [4]. $BaSi_2$ has a very large absorption coefficient (α) of 3×10^4 cm^{-1} at 1.5 eV [5], despite being an indirect bandgap semiconductor [6,7]. The conduction-band minimum and the valence-band maximum are reported to be at T(0 1/2 1/2)), and around (0 1/3 0) along the Γ-Y(0 1/2 0) direction, respectively [4,6]. The crystal structure of $BaSi_2$ has been well reported in the literature as a simple orthorhombic structure (space group Pnma) with a unit cell containing 8 Ba and 16 Si atoms, the latter of which form Si_4 tetrahedra. $BaSi_2$ can thus be considered as Zintl phase [8,9]. Both Si and Ba are abundant in the earth's crust for the formation of $BaSi_2$ thin film solar cells, and the epitaxial growth of $BaSi_2$ on a Si(111) substrate by reactive deposition epitaxy (RDE) and molecular beam epitaxy (MBE) is possible [10-12]. $BaSi_2$ matches the Si(111) face better than Si(001) with a lattice mismatch of approximately 1% [10]. The photoresponse properties of epitaxial $BaSi_2$

layers on Si(111) and polycrystalline $BaSi_2$ layers on Si(111) layers formed on SiO_2 by the Al-induced crystallization method have shown that $BaSi_2$ is a very promising material for the formation of thin-film solar devices [13,14]. Therefore, the features and advantages of $BaSi_2$ make it a candidate material for the formation of thin film solar cells. However, the fabrication of such thin film solar cells requires the fabrication of good quality *p*-*n* junction diodes, where the electric field around the *p*-*n* junction can separate the photoexcited electron-hole pairs for photovoltaic power generation [1]. According to Imai and Watanabe, substitution of Si in the $BaSi_2$ lattice is more favorable than substitution of Ba from an energetic perspective, according to first-principle calculations [15]. In line with the theoretical expectations, Sb-doped $BaSi_2$ exhibits *n*-type conductivity, while In- and Al-doped $BaSi_2$ exhibit *p*-type conductivity [16-18]. However, Ga-doped $BaSi_2$ displays *n*-type conductivity, in contrast to the theoretical prediction [16]. We reported very recently that Cu-doped $BaSi_2$ behaves as an *n*-type semiconductor [19,20], which is in agreement with the theoretical expectation [21]. However, the number of experimental reports available on impurity doping into $BaSi_2$ has been quite limited to date.

The main objective of this research work was to grow impurity (Sb, In, Ga, Al, Ag, and Cu)-doped $BaSi_2$ films by MBE and compare their electrical properties. Special emphasis was given to the temperature dependence of resistivity in the impurity-doped $BaSi_2$ films as the basis for discussion of their conduction mechanisms.

2. Experimental Procedure

An ion-pumped MBE system equipped with standard Knudsen cells was used for Ba, Sb, In, Ga, Al, Ag, and Cu, and an electron-beam evaporation source was used for Si. Electrical measurements were conducted using high-resistivity floating-zone *n*-type or *p*-type 500-μm-thick floating-zone (FZ) Si(111) (ρ=1000–6000 Ω·cm) substrates. To suppress the current flow in the FZ-Si substrates and to avoid its influence on the electrical characterizations of the impurity-doped $BaSi_2$ films, the conductivity type of the Si substrate was chosen so that the carrier type of impurity-doped $BaSi_2$ becomes different from that of the substrate, as reported previously [16-18]. After cleaning the Si(111) substrate at 850 °C for 30 min in ultrahigh vacuum, a well-developed 7×7 reflection high-energy electron diffraction (RHEED) pattern was confirmed. RHEED patterns were observed along the [1–10] azimuth of the Si(111) substrate.

MBE growth of Cu- or Ag-doped $BaSi_2$ films was carried out as follows. A 10 nm thick $BaSi_2$ epitaxial film was formed on Si(111) at 550 °C by RDE, which was then used as a template for the $BaSi_2$ overlayers. Next, Ba, Cu (or Ag), and Si were co-evaporated to form Cu (or Ag)-doped $BaSi_2$ at 600 °C by MBE. The thickness of the grown layers including the template was 230-310 nm, which was thick enough for electrical measurements of impurity-doped $BaSi_2$ films. This is because most of the depletion region stretches toward the Si substrate at the $BaSi_2$/Si *pn* junction due to a very small carrier concentration of

approximately 10^{11} $cm^{-3}$of the Si substrates.

The amount of Cu (or Ag) atoms doped in $BaSi_2$ was varied by changing the temperature of the Cu (T_{Cu}) and Ag (T_{Ag}) sources. The ratio of the Cu to Ba vapor pressure (Cu/Ba ratio) was varied from approximately 10^{-4} to 1 by changing T_{Cu} from 800 to 1200 °C. The ratio of the Ag to Ba vapor pressure (Ag/Ba ratio) was varied from approximately 10^{-5} to 1 by changing T_{Ag} from 600 to 900 °C. The Ba source temperature was fixed at around 500 °C. Sb-, In-, Ga-, and Al-doped $BaSi_2$ films were also prepared for transport studies using various source temperatures. Details on the procedures for the MBE growth of Sb-, In-, Al-, and Ga-doped $BaSi_2$ films have been reported elsewhere [16-18]. Table 1 summarizes the carrier types and carrier concentrations in the impurity-doped $BaSi_2$ films used for the transport studies. The conductivity type of the Si substrates and the temperatures of impurity sources were also described. One sample was selected from each impurity-doped $BaSi_2$ film, as shown in Table 1, and the temperature dependence of resistivity was measured at temperatures between 20 and 300 K. In order to clarify the influence of the high-resistive thick (500 μm) FZ-Si substrates on the measured electrical properties of impurity-doped $BaSi_2$ films, we also fabricated silicon-on-insulator (SOI) substrates with approximately 0.7-μm-thick Si layers with a (111) orientation. Here, the SOI substrate was formed by bonding together the *n*-FZ-Si(111) substrate (ρ=1000–6000 Ω·cm) and a quarts substrate. Following bonding, the Si substrate was thinned to approximately 0.7 μm by grinding mechanically and by chemical

mechanical polishing processes. Detailed procedure of MBE growth of $BaSi_2$ films on the SOI substrate was already reported elsewhere [22]. Here, we formed Al-doped *p*-type $BaSi_2$ films on the *n*-type SOI substrate with T_{Al}=850 °C (sample G).

The crystal quality of the grown layers was characterized using X-ray diffraction (XRD; Rigaku RAD.) using Cu K_α X-ray and RHEED. For electrical measurement, 1 mm diameter Au/Cr electrodes were evaporated on the sample film. The carrier type, carrier concentration and mobility were characterized using approximately 5-mm-squared samples by Hall measurements using the van der Pauw method. A magnetic field of approximately 0.2 T was applied normal to the sample surface.

3. Results and Discussion

3.1 Crystallinity

Figure 1 shows θ-2θ XRD patterns of Cu-doped $BaSi_2$ films grown at T_{Cu}=800-1200 °C. The diffraction peaks of (100)-oriented $BaSi_2$, such as (200), (400) and (600), are dominant in the θ-2θ XRD patterns, matching the epitaxial relationship between $BaSi_2$ and Si for the samples grown at T_{Cu}=800 and 975 °C. The RHEED patterns included in Fig. 1 are spotty or streaky, which indicates that samples with *a*-axis oriented $BaSi_2$ were grown. However, increasing the Cu temperature resulted in a decrease in intensity of the (100)-oriented peaks, and several other diffraction peaks other than those of (100)-oriented

$BaSi_2$ became pronounced. The RHEED patterns changed from ring to halo when T_{Cu} was further increased from 1000 to 1200 °C. These results indicate that Cu doping deteriorates the crystalline quality of the grown layers.

Figure 2 shows θ-2θ XRD patterns of Ag-doped $BaSi_2$ films at T_{Ag}=600-900 °C. The diffraction peaks of (100)-oriented $BaSi_2$, such as (200), (400) and (600), are dominant in the θ-2θ XRD patterns, and other diffraction peaks other than those of (100)-oriented $BaSi_2$ are negligibly small, except for sample grown at T_{Ag}=900 °C. The RHEED patterns changed from ring to halo when T_{Ag} was increased from 800 to 900 °C, which indicates that Ag doping also deteriorates the crystalline quality of the grown layers.

Figure 3 presents θ-2θ XRD patterns for the Sb-, In-, Ga-, and Al-doped $BaSi_2$ films grown for transport studies with the source temperatures indicated. The diffraction peaks of (100)-oriented $BaSi_2$ are dominant in the θ-2θ XRD patterns. Details on the dependence of θ-2θ XRD patterns on the growth conditions of Sb-, In-, Ga-, and Al-doped $BaSi_2$ films have been reported previously [16-18].

3.2 Electrical properties of impurity-doped $BaSi_2$

As a beginning, we examined the results on Al-doped $BaSi_2$ films on the *n*-type SOI substrate. Since the resistance of the 0.7-μm-thick *n*-Si layers on the SOI substrate is approximately 700 times greater than that of the 500-μm-thick *n*-type FZ-Si, we would expect to see differences among the samples if the influence of current flow in the *n*-Si substrate is

significant. As shown in Table 1, the difference in the measured hole concentrations between samples D and G is small. It is true that we cannot exclude all the influences of the 500-μm-thick FZ-Si substrate on the measured values in samples A-E; however it is reasonable to suppose that the influence is not so significant that the conduction mechanism discussed later is valid.

Figures 4(a)-4(e) show the carrier mobility as a function of the carrier concentration for Sb-, In-, Ga-, Ag-, and Cu-doped $BaSi_2$ films measured at RT, respectively. The electrical properties of Sb-, In- and Ga-doped $BaSi_2$ have already been reported [16,17]. The hole concentration in Al-doped $BaSi_2$ remained almost unchanged regardless of different T_{Al} [18]. Figures 4(a)-4(c) are presented for comparison with those of Cu- and Ag-doped $BaSi_2$. Undoped $BaSi_2$ exhibits *n*-type conductivity, where the electron density is approximately 5×10^{15} cm^{-3} and the carrier mobility is 820 $cm^2/V\cdot s$ at RT [7]. Sb- and Ga-doped $BaSi_2$ exhibit *n*-type conductivity, while In-doped $BaSi_2$ exhibits *p*-type conductivity. The electron and hole concentrations can be controlled gradually by changing the source temperature of Sb and In, respectively. The carrier mobility decreases with increasing hole (or electron) concentration for the *p* (or *n*)-type In (or Sb)-doped $BaSi_2$. This trend is usually predicted by ionized impurity scattering in conventional semiconductors, as given by Matthiessen's rule:

$$1/\mu = 1/\mu_I + 1/\mu_L, \qquad (1)$$

where μ_I and μ_L are the carrier mobility limited by impurity and lattice scattering,

respectively.

A similar trend was also observed for the Ga-, Ag- and Cu-doped $BaSi_2$ samples; however, there is a significant difference between Sb- or In-doped $BaSi_2$ and Ga-, Ag-, or Cu-doped $BaSi_2$. As shown in Fig. 4(c), the electron concentration in Ga-doped $BaSi_2$ increased significantly from 10^{16} to more than 10^{20} cm^{-3}, which indicates that control of the electron concentration in $BaSi_2$ is difficult to achieve by Ga doping. The same tendency was observed for Cu-doped $BaSi_2$, as shown in Fig. 4(e). In the case of Ag-doped $BaSi_2$, the hole concentration remained almost unchanged like in Al-doped $BaSi_2$, regardless of different T_{Ag}, which indicates that control of the hole concentration in $BaSi_2$ is not easily achieved by Ag doping. It should also be noted that Ag-doped $BaSi_2$ exhibits *p*-type conductivity, while Cu-doped exhibits *n*-type conductivity, although Ag and Cu are isoelectric atoms. According to Imai and Watanabe, Cu atoms are likely to occupy interstitial sites in $BaSi_2$ rather than substitutional sites, due to their small atomic radius [21]. Our claim, based on the experimental results, that the doping of Cu into $BaSi_2$ gives rise to *n*-type $BaSi_2$, is consistent with their theoretical prediction [21].

The conduction mechanism can be investigated from the temperature dependence of resistivity ρ, of impurity-doped $BaSi_2$ films. Table 1 summarizes the preparation of samples for this purpose. One sample was used from each impurity-doped $BaSi_2$ film. In general, at low temperatures, carriers in a system having disorder caused by, for example, impurity

doping are thought to hop from one impurity atom to the next, and the Coulomb potential around the impurity atom is overcome by means of thermal energy. The conductivity in such a system is determined by a hopping transport, where the resistivity ρ has been found to follow the law, $\log\rho \propto \left(T^*/T\right)^{1/q}$, where T^* is the characteristic temperature, and q is the parameter determining the Mott-type (q=2) or the Shklovskii-Efros (SE) type (q=4) variable-range hopping (VRH) conduction [23-26]. Figures 5(a)-5(f) show the logarithmic dependence of resistivity on both $1/T^{1/2}$ and $1/T^{1/4}$ for Sb-, In-, Ga-, Al-, Ag-, and Cu-doped $BaSi_2$, respectively. Non-linear behavior is observed for Sb- and In-doped $BaSi_2$, as shown in Figs. 5(a) and (b). In contrast, the linear behavior evident in Figs. 5(c)-(f) indicates that the carrier transport in the films can be explained by VRH conduction. On the basis of these results, we conclude that VRH conductions occur in Ga-, Al-, Ag-, and Cu-doped $BaSi_2$. However, both types of VHR explained relatively well the temperature dependence of conductivities in Ga-, Al- Ag- and Cu-doped $BaSi_2$, which suggests that there is a certain amount of defect levels in the forbidden energy gap. This explains why the carrier concentration cannot be controlled by impurity doping in Ga-, Al-, Ag- and Cu-doped $BaSi_2$ films, as demonstrated by the results shown in Figs. 4(c)-4(e). We cannot say for certain at present which of the SE-type or the Mott-type VRH conduction better describes the film properties. The transition from Mott-type to SE-type VRH was observed in polycrystalline β-$FeSi_2$ films with lowering temperature

[27]. Thus, electrical characterizations at much lower temperatures will give us information about this.

4. Conclusions

Impurity (Sb, In, Cu, Al, Ga, and Ag)-doped $BaSi_2$ films were grown by MBE and their electrical properties were measured. Sb-, Cu- and Ga-doped $BaSi_2$ exhibited *n*-type conductivity, while In-, Al-, and Ag-doped $BaSi_2$ exhibited *p*-type conductivity. The temperature dependence of resistivity indicated that the carrier transport in Ga-, Al-, Cu-, and Ag-doped $BaSi_2$ can be well explained by both SE-type and Mott-type VRH conduction.

Acknowledgements

This work was supported in part by Core Research for Evolutional Science and Technology (CREST) of the Japan Science and Technology Agency. We would like to thank Dr. Mitsushi Suzuno for the helpful discussions and valuable comments during the course of this research.

[1] S.M. Sze. *Semiconductor devices; Physics and Technology*, 2nd Edition (2001).

[2] C.H. Henry, J. Appl. Phys. 51 (1980) 4494.

[3] K. Morita, Y. Inomata, T. Suemasu, Jpn. J. Appl. Phys. 45 (2006) L390.

[4] Y. Imai, A. Watanabe, Thin Solid Films 515 (2007) 8219.

[5] K. Toh, T. Saito, T. Suemasu, Jpn. J. Appl. Phys. 50 (2011) 068001.

[6] D.B. Migas, V.L. Shaposhnikov, V.E. Borisenko, Phys. Status Solidi B 244 (2007) 2611.

[7] K. Morita, Y. Inomata, T. Suemasu, Thin Solid Films 508 (2006) 363.

[8] J. Evers, G. Oehlinger, A. Weiss, Angew. Chem., Int. Ed. 16 (1977) 659.

[9] M. Imai, T. Hirano, J. Alloys Compd. 224 (1995) 111.

[10] R.A. McKee, F.J. Walker, J.R. Conner, R. Raj, Appl. Phys. Lett. 63 (1993) 2818.

[11] Y. Inomata, T. Nakamura, T. Suemasu, F. Hasegawa, Jpn. J. Appl. Phys. 43 (2004) L478.

[12] Y. Inomata, T. Nakamura, T. Suemasu, F. Hasegawa, Jpn. J. Appl. Phys. 43 (2004) 4155.

[13] Y. Matsumoto, D. Tsukada, R. Sasaki, M. Takeishi, T. Suemasu, Appl. Phys. Express 2 (2009) 021101.

[14] D. Tsukada, Y. Matsumoto, R. Sasaki, M. Takeishi, T. Saito, N. Usami, T. Suemasu, Appl. Phys. Express 2 (2009) 051601.

[15] Y. Imai, A. Watanabe, Intermetallics 15 (2007) 1291.

[16] M. Kobayashi, K. Morita, T. Suemasu, Thin Solid Films 515 (2007) 8242.

[17] M. Kobayashi, Y. Matsumoto, Y. Ichikawa, D. Tsukada, T. Suemasu, Appl. Phys. Express 1 (2008) 051403.

[18] M. Takeishi, Y. Matsumoto, R. Sasaki, T. Saito, T. Suemasu, Physics Procedia 11 (2011) 27.

[19] M. Ajmal Khan, M. Takeishi, Y. Matsumoto, T. Saito, and T. Suemasu, Physics Procedia 11 (2011) 11.

[20] M. Ajmal Khan, T. Saito, M. Takeishi, T. Suemasu, Advanced Materials Research (Advanced Materials for Applied Science and Technology) 326 (2011) 139.

[21] Y. Imai, A. Watanabe, Intermetallics 19 (2011) 1102.

[22] K. Toh, T. Saito, T. Suemasu, Jpn. J. Appl. Phys. 50 (2011) 068001.

[23] A. L. Efros, B.I. Shklovskii, J. Phys. C8 (1975) L49.

[24] A. L. Efros, J. Phys. C: Solid State Phys. 9 (1976) 2021.

[25] K. Yamaguchi, H. Tomioka, T. Yui, T. Suemasu, K. Ando, R. Yoshizaki, F. Hasegawa, Phys. Status Solidi C 2 (2005) 2488.

[26] E. Arushanov, K.G. Lisunov, H. Vinzelberg, G. Behr, J. Schumann, O.G. Schmidt, J. Appl. Phys. 104 (2008) 053720.

[27] K. G. Kinsunov, E. K. Arushanov, Ch. Kloc, U. Malang, E. Bucher, Phys. Stat. Sol. B 195 (1996) 227.

Figure Captions

Fig. 1. θ-2θ XRD and RHEED patterns of Cu-doped $BaSi_2$ samples grown at T_{Cu}=800-1200 °C.

Fig. 2. θ-2θ XRD and RHEED patterns of Ag-doped $BaSi_2$ samples grown at T_{Ag}=600-900 °C.

Fig. 3. θ-2θ XRD patterns of Sb-, Ga-, In-, and Al-doped $BaSi_2$ samples prepared with different impurity source temperatures for transport studies.

Fig. 4. Carrier mobility vs. carrier concentration for (a) Sb-doped *n*-type, (b) In-doped *p*-type, (c) Ga-doped *n*-type, (d) Ag-doped *p*-type, and (e) Cu-doped *n*-type $BaSi_2$ films measured at RT. The amount impurity atoms were changed by source temperatures.

Fig. 5. Logarithmic dependence of resistivity on $1/T^{1/2}$ and $1/T^{1/4}$ for (a) Sb-doped *n*-type, (b) In-doped *p*-type, (c) Ga-doped *n*-type, (d) Al-doped *p*-type, (e) Ag-doped *p*-type and (f) Cu-doped *n*-type $BaSi_2$ films.

Table 1 Carrier type and concentration of impurity (Sb, In, Ga, Al, Ag, and Cu)-doped $BaSi_2$ films, carrier type of Si substrate, and temperature of impurity sources, *T*, are indicated.

Sample	Impurity	Substrate	Carrier type	*T* (°C)	Carrier concentration at RT (cm^{-3})
A	Sb	*p*	*n*	250	3×10^{16}
B	In	*n*	*p*	650	2×10^{17}
C	Ga	*p*	*n*	700	1×10^{16}
D	Al	*n*	*p*	850	7×10^{16}
E	Ag	*n*	*p*	800	3×10^{16}
F	Cu	*p*	*n*	1000	1×10^{19}
G	Al	*n*	*p*	850	4×10^{16}

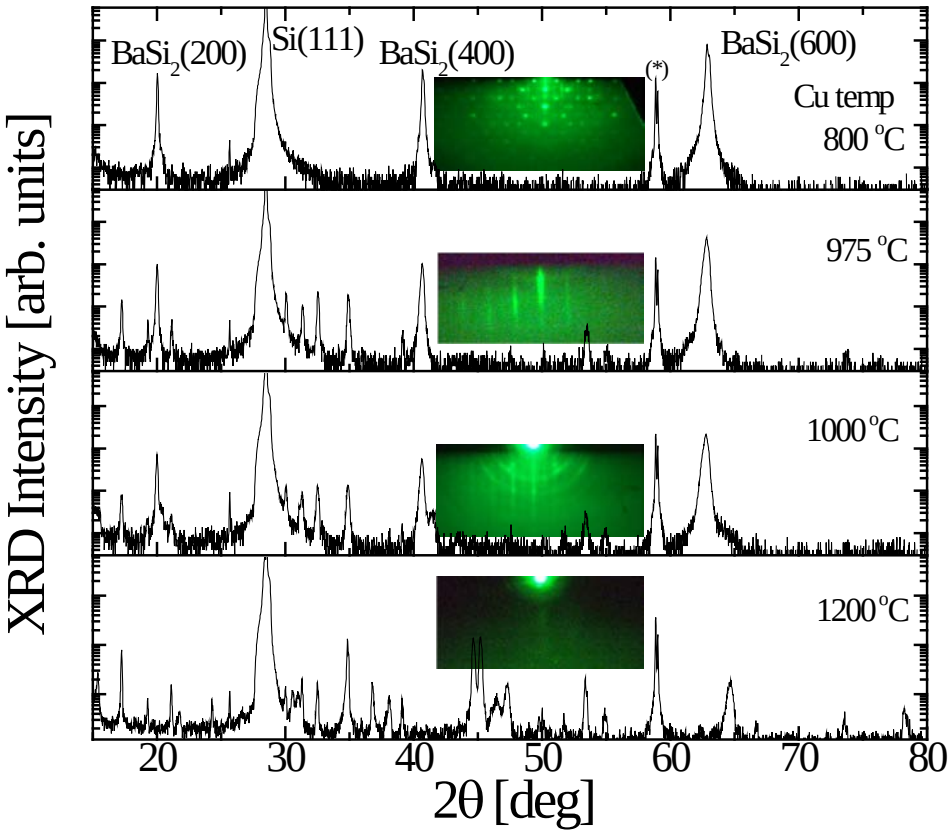
BaSi2(200)
Si(111)
BaSi2(400)
(*)
BaSi2(600)
Cu temp
800 °C
975 °C
1000 °C
1200 °C
XRD Intensity [arb. units]
20
30
40
50
60
70
80
2θ [deg]

Fig. 1

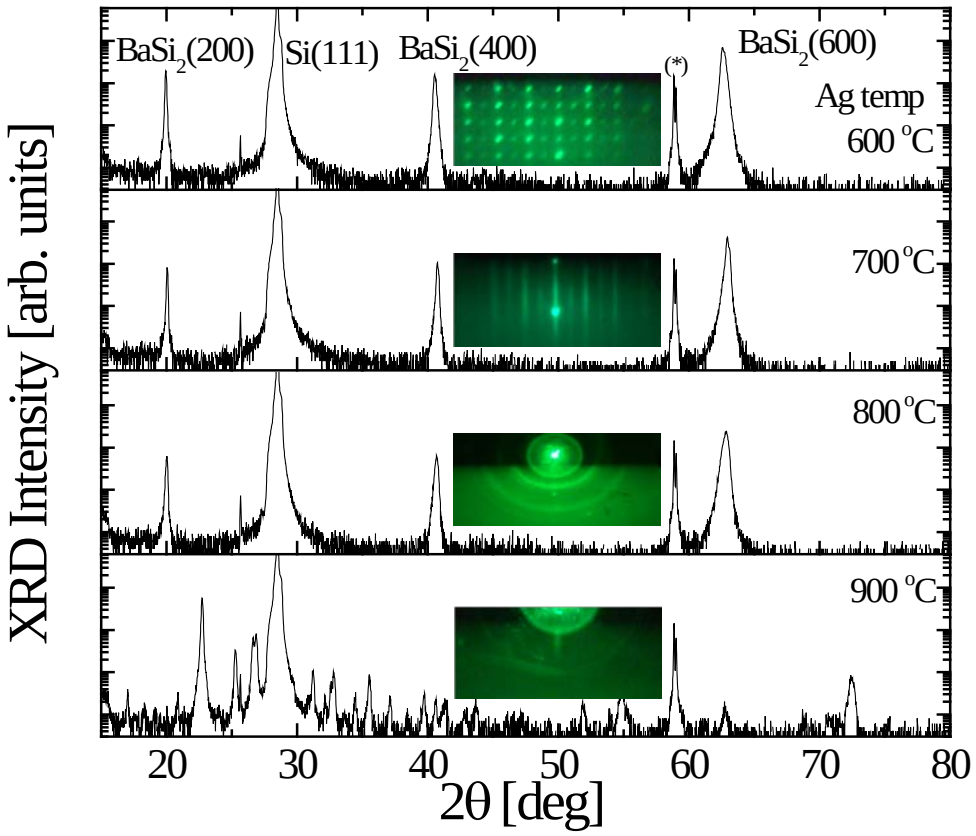
BaSi2(200)
Si(111)
BaSi2(400)
(*)
BaSi2(600)
Ag temp
600 °C
700 °C
800 °C
900 °C
XRD Intensity [arb. units]
20
30
40
50
60
70
80
2θ [deg]

Fig. 2

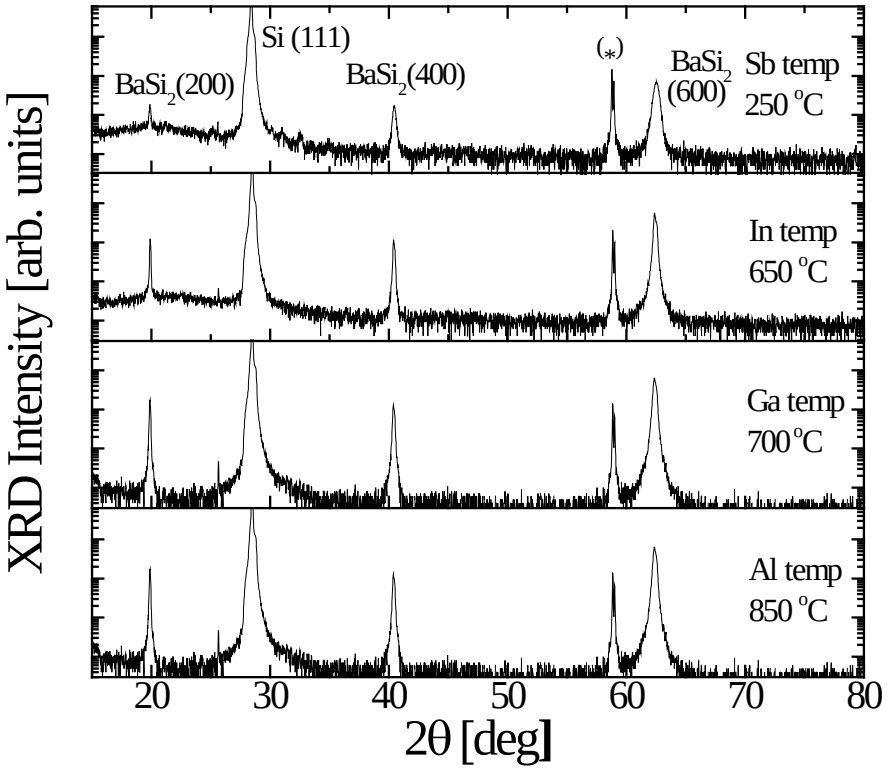
XRD Intensity [arb. units]
BaSi2(200)
Si (111)
BaSi2(400)
(*)
BaSi2 (600)
Sb temp 250 °C
In temp 650 °C
Ga temp 700 °C
Al temp 850 °C
20
30
40
50
60
70
80
2θ [deg]

Fig.3

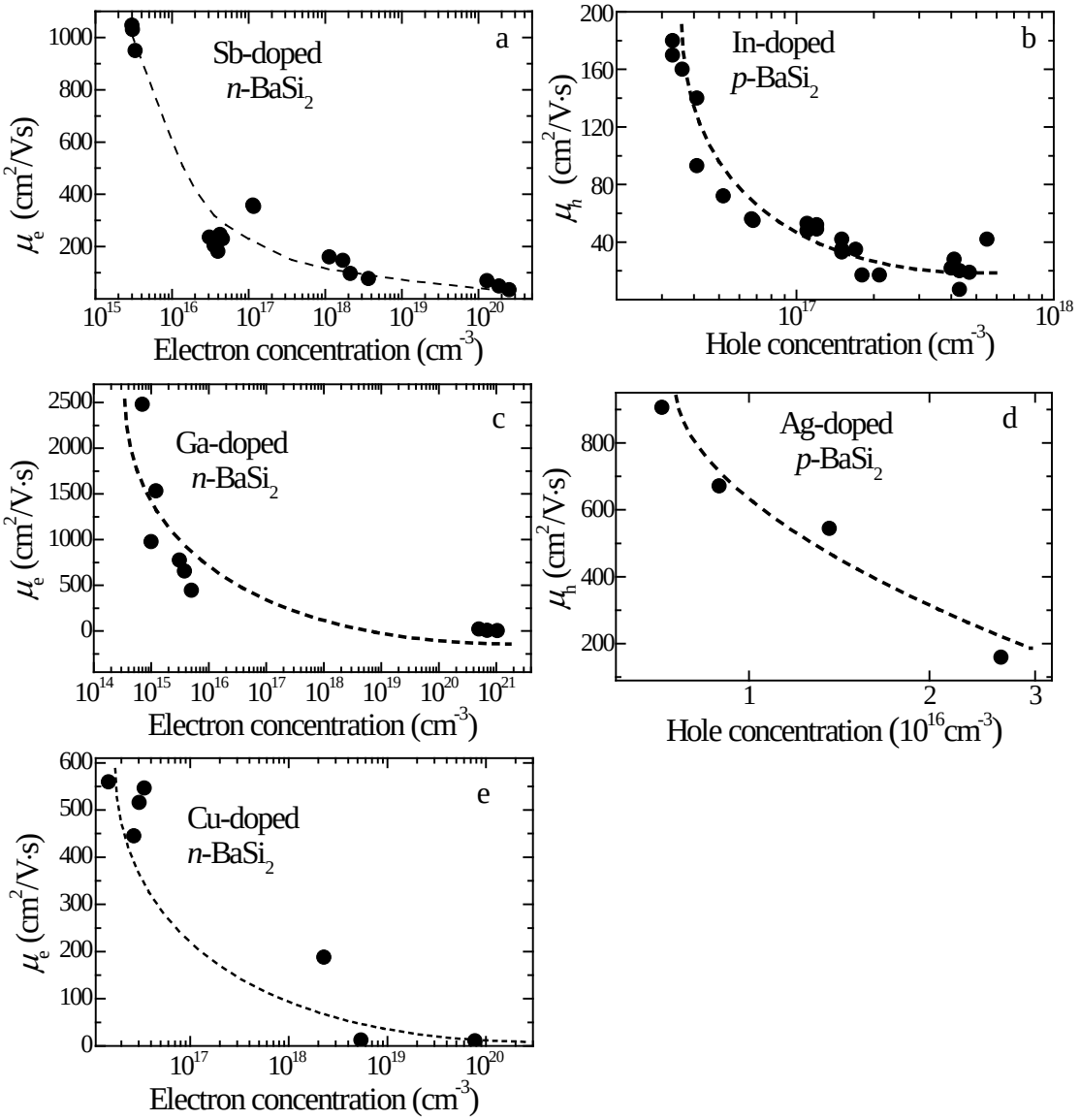
Sb-doped
n-BaSi2
a
μe (cm2/Vs)
Electron concentration (cm-3)
In-doped
p-BaSi2
b
μh (cm2/V·s)
Hole concentration (cm-3)
Ga-doped
n-BaSi2
c
μe (cm2/V·s)
Electron concentration (cm-3)
Ag-doped
p-BaSi2
d
μh (cm2/V·s)
Hole concentration (10^16 cm-3)
Cu-doped
n-BaSi2
e
μe (cm2/V·s)
Electron concentration (cm-3)

Fig. 4

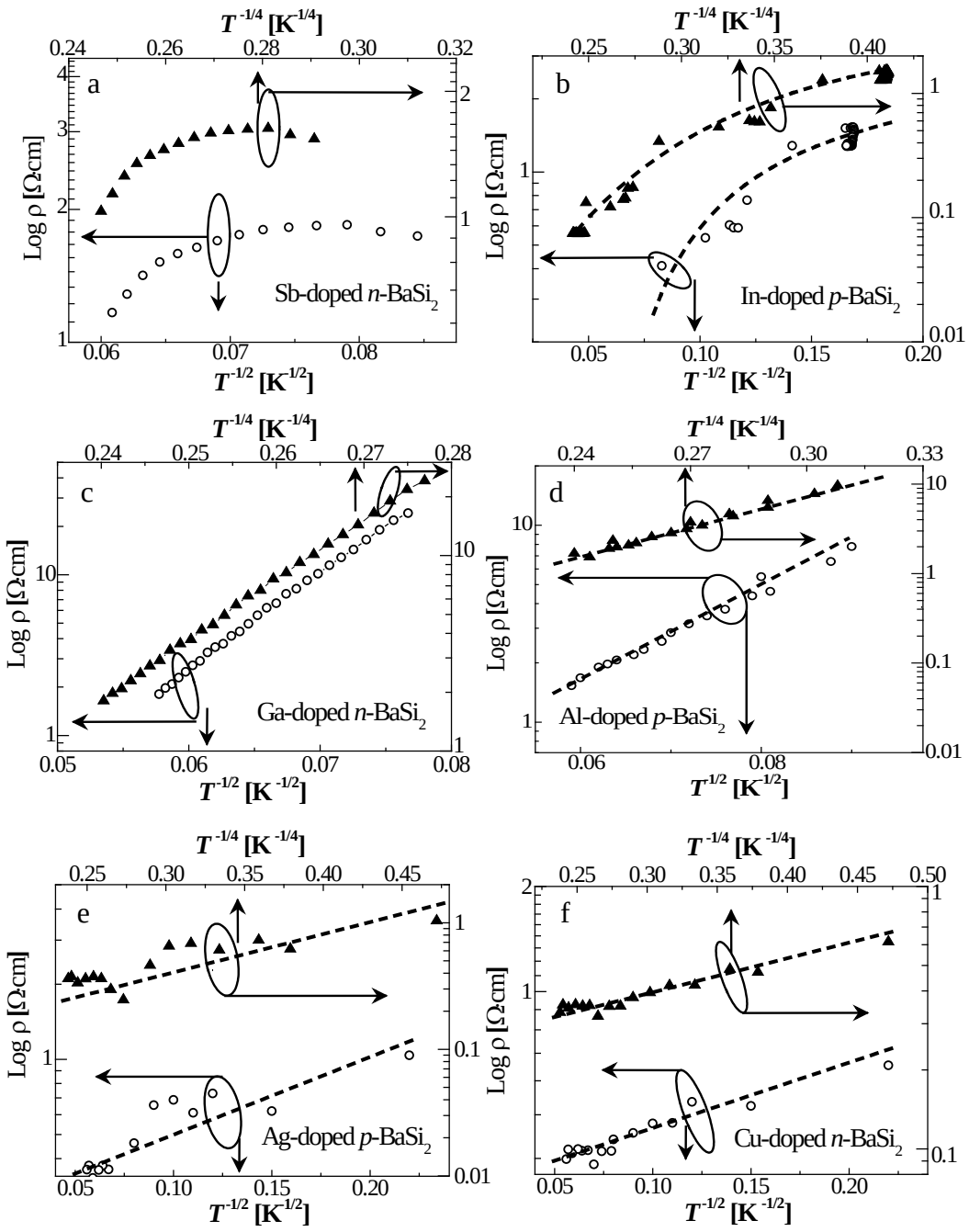
a
Sb-doped n-BaSi2
b
In-doped p-BaSi2
c
Ga-doped n-BaSi2
d
Al-doped p-BaSi2
e
Ag-doped p-BaSi2
f
Cu-doped n-BaSi2
Log ρ [Ωcm]
T -1/4 [K-1/4]
T -1/2 [K-1/2]

Fig. 5